

Schrödinger equation in the space with cylindrical geometric defect and possible application to multi-wall nanotubes

Guilherme de Berredo-Peixoto^(a), Mikhail O. Katanaev^(b),
Elena Konstantinova^(a,c) and Ilya L. Shapiro^(a)

(a) *Departamento de Física, Universidade Federal de Juiz de Fora,
Juiz de Fora, CEP 36036-330, MG, Brazil*

(b) *Steklov Mathematical Institute, Gubkin St. 8, Moscow, 119991, Russia*

(c) *Instituto Federal de Educação, Ciência e Tecnologia do Sudeste de Minas Gerais
(IFSEMG), Juiz de Fora, CEP 36080-001, MG, Brazil*

Abstract

The recently invented cylindrical geometric space defect is applied to the electron behaviour in the system which can be regarded as a simplified model of a double-wall nanotube. By solving the Schrödinger equation in the region of space with cylindrical geometric defect we explore the influence of such geometric defect on the energy gap and charge distribution. The effect is qualitatively similar to the one obtained earlier by means of traditional simulation methods. In general, the geometric approach can not compete with the known methods of theoretical study of the nanostructures, such as molecular dynamics. However it may be useful for better qualitative understanding of the electronic properties of the nanosystems.

1 Introduction

The theory of defects is an important part of the mathematical physics. In particular, topological defects attract much attention in modern condensed matter physics (see, e.g., [1, 2] for an introduction and recent review). Another elegant approach in this area is the geometric theory of defects [3, 4] (see also [5] for the introduction), which is formulated in terms of the notions originally developed in the theories of gravity. The main kinds of defects which were described in the framework of Riemann-Cartan geometry are dislocations and disclinations. This means that the curvature and torsion tensors are interpreted as surface densities of Frank and Burgers vectors and thus linked to the nonlinear, generally inelastic deformations of a solid. Recently, the qualitatively new kind of geometric defect corresponding to the cylindrical geometry has been described in [6]. In the framework of

geometric approach, the static massive thin cylindrical shells are considered as sources in Einstein equations. It turns out that these defects correspond to δ - and δ' -function type energy-momentum tensors. It would be interesting to find some useful applications of this new kind of defect. One may think about cosmological applications and/or about the condensed matter physics applications, which can be not infinitely far from each other [7].

One of the natural question to address is in which way the new kind of defects can be applied to the condensed matter physics? In this respect we can mention, for example, the recent works [8, 9] devoted to the cylindrical nanoparticles in a liquid crystal solvent. It would be interesting to see whether the cylindric defects can be useful in description of these systems. However, at the first place, the cylindrical geometry is associated with the nanotubes (see, e.g., [11, 10, 12, 13] for the general review). As we shall see in what follows, the most appropriate object of our interest would be not the usual single-wall nanotubes but the double-wall nanotubes (DWNTs) or, more general, multi-wall nanotubes (MWNTs).

The MWNTs attract great attention [14, 15, 16], in particular due to higher temperature stability and stiffness compared to the similar single-wall nanotubes. The inner and the outer layers of the DWNTs can be metallic (M) or semiconductor (S). Correspondingly, there are DWNTs of different kinds, namely: semiconductor-semiconductor (S/S case), metal-semiconductor (M/S case), semiconductor-metal (S/M case) and metal-metal (M/M case). It has been emphasized recently in [17] that the M/M type of the DWNTs is the most difficult to meet, but, at the same time, this particular configuration is especially interesting to explore. Let us note that there are some theoretical and experimental data available on the energy gap of a MWNTs compared to the purely metallic tubes [18] (see also [15]).

In the present work we shall consider how the cylindrical geometric defects can be related to the theoretical investigation of the M/M type DWNTs. Our approach will be to consider the solution of the one-particle Schrödinger equation in the space with the cylindrical geometric defect. Let us note that the idea to explore the one-particle Schrödinger equation as a way to describe nanotubes is not completely new. One can mention, e.g., the work of Ref. [19], where a nonrelativistic spinless particle moving in a cylindrical surface (also in a thick cylindrical hollow) is investigated. On the other side, there are also publications on quantized particles moving in a curved background, with or without defects. Many of them address the problem of a test particle in a spacetime with cosmic strings and are motivated by the corresponding cosmological models. Also, in Ref. [20], for example, the Schrödinger picture description of vacuum states is studied and applied to simple cosmological models without cosmic strings.

An important difference between the works mentioned above and our approach is that we do not consider the cylindrically symmetric potential. Instead, we consider the free

Schrödinger equation (without potential) in the space with the cylindrical geometric defect. In order to see in which situation this method may be more natural, let us present the following observations. The conventional nanotubes are compounds where the electron can propagate only on the tube surface and not in the three-dimensional bulk. In the case of DWNTs there are two distinct conducting cylindrical shells. If we consider the electron in such system, the tube or space division shell between the two tubes is unlikely to create an electromagnetic potential difference between the two conducting layers while being essential for the electronic properties of the compound. Therefore, the presence of the division between the two shells fits the geometric defect case described in [6], so it looks natural to perform some investigation of the corresponding quantum systems.

It is necessary to mention some recent publications motivated by condensed matter applications of geometric approach. In Ref. [21], the effect of curvature is analyzed in particle scattering. Concerning the problems in the presence of defects, we can also mention, e.g., Ref. [22], where a particle which moves in a magnetic field in a space with disclination and screw dislocation has been studied. Also, the paper [23] explores the bounded states of an electric dipole in the presence of a conical defect. Despite our work can be seen as continuation of this line, we consider a rather different approach to the geometrical defects [6].

Indeed, there are well-known methods for calculating electronic and mechanic properties for different compounds, $3D$, $2D$ or $1D$ nanosystems, in particular. For example, using the density functional (DFT) - based methods we can explore different systems (including periodical ones), and one obtains the desirable results with high precision [24]. At the same time, it looks interesting to have an alternative, more simple (albeit potentially reliable) approach which could permit us to obtain important qualitative information, and maybe also help in qualitative understanding, e.g., of the electronic properties of the mentioned systems. In what follows we shall develop relatively simple and to great extent analytic method based on the geometric theory of defects. As we shall see in brief, this approach looks justified, for it enables one to arrive at the qualitative understanding of the origin of modifications of energy gaps and density distribution due to the presence of the defect shell between the conducting layers.

The paper is organized as follows. In the next two sections we present a brief but to some extent pedagogical description of the tube dislocation in the linear elasticity theory and in the geometric theory of defects. Despite the content of these sections is essentially the same as the one of [6], we include it here for the sake of completeness. In section 4 we consider the Schrödinger equation and describe the results of its numerical solution. In particular, we compare the energy levels and charge density distributions of the MWNTs with the ones of the similar cylindrical tube without defect (it can be obtained analytically) and

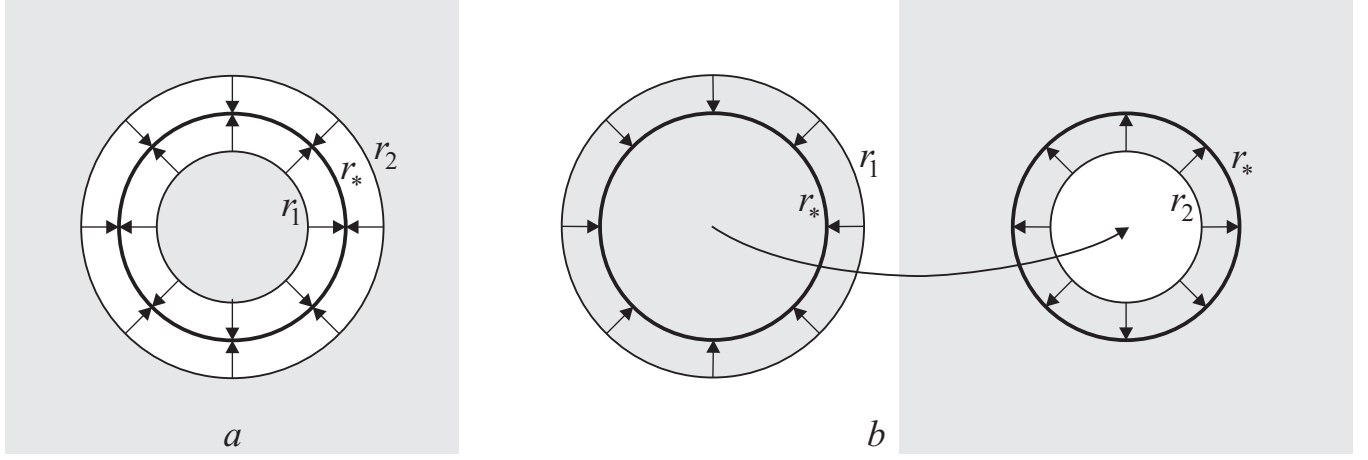


Figure 1: Negative (a) and positive (b) tube dislocations.

with the established earlier features of the energy spectrum of the system [15, 18]. Finally, in section 5 we draw our conclusions.

2 Tube dislocation in the linear elasticity theory

Let us start by describing the tube dislocations in the simplest case of linear elasticity theory. Consider a homogeneous and isotropic elastic media as a three-dimensional Euclidean space \mathbb{R}^3 with Cartesian coordinates x^i, y^i , where $i = 1, 2, 3$. The Euclidean metric is denoted by $\delta_{ij} = \text{diag}(+++)$. The basic variable in the elasticity theory is the displacement vector of a point in the elastic media, $u^i(x)$, $x \in \mathbb{R}^3$. In the absence of external forces, Newton's and Hooke's laws reduce to three second order partial differential equations which describe the equilibrium state of elastic media (see, e.g., [25]),

$$(1 - 2\sigma)\Delta u_i + \partial_i \partial_j u^j = 0. \quad (1)$$

Here Δ is the Laplace operator and the dimensionless Poisson ratio σ ($-1 \leq \sigma \leq 1/2$) is defined as

$$\sigma = \frac{\lambda}{2(\lambda + \mu)}.$$

λ and μ are called the Lamé coefficients, they characterize the elastic properties of media.

Raising and lowering of Latin indices i, j, \dots can be done by using the Euclidean metric, δ_{ij} , and its inverse, δ^{ij} . Eq. (1) together with the corresponding boundary conditions enables one to establish the solution for the field $u^i(x)$ in a unique way.

Let us pose the problem for the tube dislocation shown in Figure 1, a.

This tube dislocation can be produced as follows. We cut out the thick cylinder of media located between two parallel cylinders of radii r_1 and r_2 ($r_1 < r_2$) with the axis $z = x^3$ as the symmetry axis of both cylinders, move symmetrically both cutting surfaces one to the other and finally glue them. Due to circular and translational symmetries of the problem, in the equilibrium state the gluing surface is also the cylinder, of the radius r_* which will to be found below.

Within the procedure described above and shown in Fig.1,*a* we observe the negative tube dislocation because part of the media was removed. This corresponds to the case of $r_1 < r_2$. However, the procedure can be applied in the opposite way by addition of extra media to \mathbb{R}^3 as shown in Fig.1,*b*. In this case, we meet a positive tube dislocation and the inequality has an opposite sign, $r_1 > r_2$. It is important to note that the approach adopted here above concerns our treatment of the division of the shells of the DWNT as a geometric defect. Of course, it can not be seen as a practical prescription for building nanotubes of other objects.

Let us start by calculating the radius of the equilibrium configuration r_* . This problem is naturally formulated and solved in cylindrical coordinates r, φ, z . Let us denote the displacement field components in these coordinates by u^r, u^φ, u^z . In our case, $u^\varphi = u^z = 0$ due to the symmetry of the problem, so that the radial displacement field $u^r(r)$ can be simply denoted as $u^r(r) = u(r)$.

The boundary conditions for the equilibrium tube dislocation are

$$u|_{r=0} = 0, \quad u|_{r=\infty} = 0, \quad \left. \frac{du_{\text{in}}}{dr} \right|_{r=r_*} = \left. \frac{du_{\text{ex}}}{dr} \right|_{r=r_*}. \quad (2)$$

The first two conditions are purely geometrical, and the third one means the equality of normal elastic forces inside and outside the gluing surface in the equilibrium state. The subscripts “in” and “ex” denote the displacement vector field inside and outside the gluing surface, respectively.

Let us note that our definition of the displacement vector field follows [5], but differs slightly from the one used in many other references. In our notations, the point with coordinates y^i , after elastic deformation, moves to the point with coordinates x^i :

$$y^i \rightarrow x^i(y) = y^i + u^i(x). \quad (3)$$

The displacement vector field is the difference between new and old coordinates, $u^i(x) = x^i - y^i$. Indeed, we are considering the components of the displacement vector field, $u^i(x)$, as functions of the final state coordinates of media points, x^i , while in other references they are functions of the initial coordinates, y^i . The two approaches are equivalent in the absence of dislocations because both sets of coordinates x^i and y^i cover the entire Euclidean space \mathbb{R}^3 . On the contrary, if dislocation is present, the final state coordinates x^i cover the

whole \mathbb{R}^3 while the initial state coordinates cover only part of the Euclidean space lying outside the thick cylinder which was removed. For this reason the final state coordinates represent the most useful choice here.

The elasticity equations (1) can be easily solved for the case of tube dislocation under consideration. The Laplacian and the divergence in the cylindrical coordinates have the form

$$\Delta u_r = \frac{1}{r} \partial_r (r \partial_r u_r) + \frac{1}{r^2} \partial_\varphi^2 u_r + \partial_z^2 u_r - \frac{1}{r^2} u_r - \frac{2}{r^2} \partial_\varphi u_\varphi, \quad (4)$$

$$\partial_i u^i = \frac{1}{r} \partial_r (r u^r) + \frac{1}{r} \partial_\varphi u^\varphi + \partial_z u^z, \quad (5)$$

where the indices are lowered using the Euclidean metric in cylindrical coordinates, $u_r = u^r$, $u_\varphi = u^\varphi r^2$ and $u_z = u^z$. Let us note that the last two terms in (4) are due to the geometric covariant nature of the Laplace operator, which is constructed on the basis of covariant derivatives.

One can remember that only the radial component differs from zero. The angular φ and z components of equations (1) are identically satisfied, and the radial component reduces to the ordinary differential equation,

$$\partial_r \left[\frac{1}{r} \partial_r (r u) \right] = 0, \quad (6)$$

which has a general solution

$$u = ar - \frac{b}{r},$$

depending on the two arbitrary constants of integration a and b . Due to the first two boundary conditions (2), the solutions inside and outside the gluing surface are

$$\begin{aligned} u_{\text{in}} &= ar, & a > 0, \\ u_{\text{ex}} &= -\frac{b}{r}, & b > 0. \end{aligned} \quad (7)$$

The signs of the integration constants correspond to the negative tube dislocation shown in Fig.1,*a*. For positive tube dislocation, Fig.1,*b*, both integration constants have opposite signs, $a < 0$ and $b < 0$.

Using the solution (2) and the third boundary condition (2), one can determine the radius of the gluing surface,

$$r_*^2 = \frac{b}{a}. \quad (8)$$

After simple algebra the integration constants can be expressed in terms of the initial radius of external and internal cylinders

$$a = \frac{r_2 - r_1}{r_2 + r_1} = \frac{l}{2r_*}, \quad b = \frac{r_2^2 - r_1^2}{4} = \frac{lr_*}{2}, \quad (9)$$

where

$$l = r_2 - r_1, \quad \text{and} \quad r_* = \frac{r_2 + r_1}{2}$$

are the thickness of the removed cylinder and the radius of the gluing surface, respectively. The first expression in (9) restricts the range of the integration constant, $0 < |a| < 1$.

It is interesting to note that the above formulas are applicable for both negative and positive tube dislocations. One has to take $l > 0$ and $l < 0$ in these cases, respectively. Indeed, the negative thickness in the last case means that, before the deformation, the external radius must be smaller than the internal one and that the proper deformation consists in inserting some matter between the cylindrical surfaces. In both cases we see that the gluing surface $r = r_*$ lies exactly in the middle between the radii r_1 and r_2 .

Finally, within the linear elasticity theory, Eq.(7) with the integration constants (9) yields a complete solution for the tube dislocation. This solution is valid for small relative displacements, when $l/r_1 \ll 1$ and $l/r_2 \ll 1$. It is remarkable that the solution obtained in the framework of linear elasticity theory does not depend on the Poisson ratio of the media. In this sense, the tube dislocation is a purely geometric defect which does not feel the elastic properties.

In order to use the geometric approach we have to present the results obtained above in other terms. For this end we compute the geometric quantities of the manifold corresponding to the tube dislocation. From the geometric point of view, the elastic deformation (3) is a diffeomorphism between the given domains in the Euclidean space. The original elastic media \mathbb{R}^3 , before the dislocation is made, is described by Cartesian coordinates y^i with the Euclidean metric δ_{ij} . An inverse diffeomorphism transformation $x \rightarrow y$ induces a nontrivial metric on \mathbb{R}^3 , corresponding to the tube dislocation. In Cartesian coordinates this metric has the form

$$g_{ij}(x) = \frac{\partial y^k}{\partial x^i} \frac{\partial y^l}{\partial x^j} \delta_{kl}.$$

We use curvilinear cylindrical coordinates for the tube dislocation and therefore it is useful to modify our notations. The indices in curvilinear coordinates in the Euclidean space \mathbb{R}^3 will be denoted by Greek letters x^μ , $\mu = 1, 2, 3$. Then the ‘‘induced’’ metric for the tube dislocation in cylindrical coordinates is¹

$$g_{\mu\nu}(x) = \frac{\partial y^\rho}{\partial x^\mu} \frac{\partial y^\sigma}{\partial x^\nu} \overset{\circ}{g}_{\rho\sigma}, \quad (10)$$

where $\overset{\circ}{g}_{\rho\sigma}$ is the Euclidean metric written in cylindrical coordinates. We denote cylindrical coordinates of a point before the dislocation is made by $\{y, \varphi, z\}$, where y without index stands for the radial coordinate and we take into account that the coordinates φ and z do

¹Note1

not change. Then the diffeomorphism is described by a single function relating old and new radial coordinates of a point $y = r - u(r)$, where

$$u(r) = \begin{cases} ar, & r < r_* \\ -\frac{b}{r}, & r > r_* \end{cases} \quad (11)$$

It is easy to see that this function has a discontinuity $ar_* + b/r_* = l$ at the point of the cut. Therefore a special care must be taken in calculating the components of induced metric. It proves useful to introduce the function

$$v = \begin{cases} a, & r \leq r_* \\ \frac{b}{r^2}, & r \geq r_* \end{cases} \quad (12)$$

which is continuous on the cutting surface. This function differs from the derivative $u'(r)$ of the displacement vector field $u(r)$ defined in (11) by the δ -function

$$u' = u'(r) = v(r) - l\delta(r - r_*). \quad (13)$$

Now we define the induced metric for the tube dislocation as

$$ds^2 = (1 - v)^2 dr^2 + (r - u)^2 d\varphi^2 + dz^2. \quad (14)$$

It is easy to check that this metric outside the cut agrees with the expression (10). The difference between the two expressions is that (14) is defined on the cutting surface while (10) is not. The volume element corresponding to (14) is

$$\sqrt{|g|} = (1 - v)(r - u), \quad \text{where } g = \det g_{\mu\nu}.$$

Let us note that the metric (14) differs from the one which results from the formal substitution of $y = r - u(r)$ into the Euclidean metric $ds^2 = dy^2 + y^2 d\varphi^2 + dz^2$ by the square of the δ -function in the g_{rr} component. This procedure is required in the geometric theory of defects, because otherwise the Burgers vector can not be expressed as the surface integral [5]. Finally, the metric component $g_{rr}(r) = (1 - v)^2$ of tube dislocation is a continuous function, and the angular component $g_{\varphi\varphi} = (r - u)^2$ has the jump at the surface of the cut.

The displacement vector field (13) and induced metric (14) represent the solution of the field equations of the linear elasticity theory (1) with the boundary conditions (2) describing tube dislocation. The solution does not depend on the elastic properties of the media due to the universality of the linear approximation.

3 Tube dislocation in the geometric theory of defects

Our next step is to go beyond the linear approximation and consider the defects in elastic media with a tube dislocation. In the geometric theory of defects [3, 4, 27, 28] (see [5] for the for review) the defects in elastic media with a spin structure are the framework of differential geometry. The main assumption is that the elastic media is a three-dimensional manifold with a Riemann-Cartan geometry. This approach enables one to treat the non-linear regime and also enables one to deal with a continuous distribution of defects. The tube dislocation in the geometric theory of defects was introduced and considered in details in Ref. [6], so here we present only a short account of the formalism.

The geometry is determined by the Einsteins equations with the source term given by the energy-momentum tensor. We remark that the formalism under discussion is diffeomorphism invariant and thus, in contrast to the linear elasticity theory, the displacement vector field does not show up explicitly in the field equations. At the same time we require that the linear approximation gives standard result. Therefore a natural choice for the energy-momentum tensor is

$$-\frac{1}{2}T_{\mu\nu} = \sqrt{|g|} \left(\tilde{R}_{\mu\nu} - \frac{1}{2}g_{\mu\nu}\tilde{R} \right), \quad (15)$$

where the curvature terms are constructed by using the metric obtained within the elasticity theory, e.g., (14) for the tube dislocation case. The straightforward calculations yeild the following relevant component of the above equation [6]:

$$T_{zz} = \frac{4lr_*}{2r_* - l} \delta'(r - r_*). \quad (16)$$

It is worth mentioning that the above calculation is non-trivial because the curvature terms contains ambiguous pieces, like δ^2 , but surprisingly they cancel in the final expression.

It turns out that the solution in the geometric theory of defects in some appropriate gauge conditions coincides exactly with the metric (14). Thus, the result obtained within the linear elasticity theory is quite general and we can adopt the corresponding geometry as a background for the quantum consideration.

4 Schrödinger equation in the presence of tube defect

Consider the quantum description of a spinless particle in the space with tube dislocation. The quantum properties of our interest are encoded into the time independent wave function, $\psi(r, \phi, z)$ which is the solution of the stationary covariant Schrödinger equation,

$$\Delta\psi = -\chi^2\psi. \quad (17)$$

Here we use the notation $\chi = \sqrt{2mE}/\hbar$, where m and E are mass and energy of the particle. Δ is the covariant Laplacian operator, given by

$$\Delta\psi = \frac{1}{\sqrt{g}}\partial_\mu(\sqrt{g}g^{\mu\nu}\partial_\nu\psi). \quad (18)$$

Notice that the wave function behaves as a scalar field when subject to covariant derivative, because the particle is spinless. For this reason (18) boils down to eq. (4) in cylindrical coordinates and, furthermore, the torsion does not couple with the wave function². The straightforward calculations lead to the following form of Schrödinger equation in the space-time with the elastic deformations described in section 2,

$$\frac{1}{(1-v)^2}\frac{\partial^2\psi}{\partial r^2} + \frac{1}{(1-v)^2}\left(\frac{1-u'}{r-u} + \frac{v'}{1-v}\right)\frac{\partial\psi}{\partial r} + \frac{1}{(r-u)^2}\frac{\partial^2\psi}{\partial\phi^2} + \frac{\partial^2\psi}{\partial z^2} = -\chi^2\psi. \quad (19)$$

In order to obtain the energy spectrum and density distribution, we need to solve the above equation separately in the two distinct regions, namely for $r < r_*$ (this implies also $y < r_1$) and for $r > r_*$ (in this case $y > r_2$). We shall denote the corresponding solutions for the wave functions as $\psi^{\text{int}}(r)$ and $\psi^{\text{ext}}(r)$. One has to take into account also the normalization and boundary conditions, along with the matching condition at $r = r_*$, namely,

$$\psi^{\text{int}}(r_*) = \psi^{\text{ext}}(r_*), \quad (20)$$

$$\left(\frac{\partial\psi^{\text{int}}}{\partial r}\right)_{r=r_*} = \left(\frac{\partial\psi^{\text{ext}}}{\partial r}\right)_{r=r_*}. \quad (21)$$

It would be very difficult to solve the equation (19) in a direct way, especially outside the tube defect. However the solution becomes rather straightforward if we perform the inverse coordinate transformation $r \rightarrow y = r - u(r)$. In this case the Schrödinger equation becomes very simple and in fact it is just the one for the free particle,

$$\frac{\partial^2\psi}{\partial y^2} + \frac{1}{y}\frac{\partial\psi}{\partial y} + \frac{1}{y^2}\frac{\partial^2\psi}{\partial\phi^2} + \frac{\partial^2\psi}{\partial z^2} = -\chi^2\psi. \quad (22)$$

After the equation (22) is solved one has to perform the coordinate mapping, that means the direct elasticity transformation in order to get the solution of the equation (19) of our interest. It is important to keep in mind that the triviality of the equation (22) does not mean the triviality of the solutions of the equation of our interest (19). The whole point is that the solutions are coordinate dependent (while the equation is covariant) and the physical results correspond to the coordinates x^i defined in eq. (3).

²Note2

The solution of the free Schrödinger equation (22) can be easily obtained via the usual method of separating variables if we consider a finite cylinder between $z = -L$ and $z = L$. We set $\psi(y, \phi, z) = \rho(y)\Phi(\phi)Z(z)$ and arrive, after replacing this form into the equation and some standard algebra, at the solutions for ϕ and z dependences,

$$\Phi(\phi) = e^{im\phi} \quad \text{and} \quad Z(z) = \cos(kz), \quad (23)$$

where $m = 0, 1, 2, \dots$ and $k = n\pi/L$ ($n = 1, 3, 5, \dots$). These solutions correspond to the boundary conditions $Z(-L) = Z(L) = 0$. The radial function satisfies the equation

$$\frac{\partial^2 \rho}{\partial y^2} + \frac{1}{y} \frac{\partial \rho}{\partial y} = - \left(\bar{\chi}^2 - \frac{m^2}{y^2} \right) \rho. \quad (24)$$

where $\bar{\chi}^2 = \chi^2 - k^2$. The general solution for the last equation has the form

$$\rho(y) = C_1 J_m(\bar{\chi}y) + C_2 Y_m(\bar{\chi}y), \quad (25)$$

where J_m and Y_m are Bessel function of the first kind and of the second kind (or Neumann function) respectively, and C_1, C_2 are arbitrary constants. The above solution can be mapped from the “old” coordinate y into physical coordinate r , as it was explained above, providing us an important information on the spectrum of the system and also on the charge density distribution. Let us discuss this in some details.

4.1 Energy levels

Let us consider the solution of Schrödinger equation for a particle confined in a thin region around the geometrical defect, say, in old coordinates, $r_0 \leq y \leq r_1$, $r_2 \leq y \leq r_3$. The two separate solutions are

$$\rho^{int}(y) = c_1 J_m(\bar{\chi}y) + c_2 Y_m(\bar{\chi}y), \quad y < r_1, \quad (26)$$

$$\rho^{ext}(y) = c_3 J_m(\bar{\chi}y) + c_4 Y_m(\bar{\chi}y), \quad y > r_2. \quad (27)$$

After the necessary mapping, $r = y + u$, we arrive at the exact solutions of the radial part of the equation (19). One should mention that a real finite-size tube does not have the symmetry along the z -axis, however one can consider a very long and thin tube and thus assume the translational z -symmetry as a good approximation. In our case this means an approximation of a large L , such that $k \simeq 0$.

Consider the mapping, which was already discussed above, in the detailed form. In what follows, we shall drop the bars and write χ instead of $\bar{\chi}$. In order to write down the solution in terms of physical coordinate, we have to impose the boundary conditions in the form

$$c_1 J_m(\chi r_0) + c_2 Y_m(\chi r_0) = c_3 J_m(\chi r_3) + c_4 Y_m(\chi r_3) = 0. \quad (28)$$

These conditions give us, immediately, $c_2 = -c_1 J_m(\chi r_0)/Y_m(\chi r_0)$ and $c_4 = -c_3 J_m(\chi r_3)/Y_m(\chi r_3)$. The last relations must be inserted on the matching condition at $r = r_*$. However, it turns out that the old matching conditions (21) are physically unacceptable, since they imply that the charge density, proportional to $\sqrt{g}|\psi|^2$, has a discontinuity at the surface r_* . Thus, the following conditions would be more appropriate:

$$r_1 |\rho(r_1)|^2 = r_2 |\rho(r_2)|^2, \quad \left. \frac{d}{dy} (y|\rho(y)|^2) \right|_{y=r_1} = \left. \frac{d}{dy} (y|\rho(y)|^2) \right|_{y=r_2}. \quad (29)$$

Here we have used the expression for the volume element in cylindric coordinates, $\sqrt{g(r)} = r$.

Unfortunately, the above conditions provide only two relations between arbitrary (complex) constants, in contrast to the equations (21), which provide four relations. Thus one should use another conditions (complex equations). The most natural choice is continuity of the covariant density $\sqrt{g}|\psi|^2$. Another condition with direct physical interpretation is the current conservation, that is the continuity of the current $\sqrt{g}J^\mu$, that means $\nabla_\mu J^\mu = 0$, where

$$J^\mu = -\frac{i\hbar}{2\pi} g^{\mu\nu} (\psi^* \partial_\nu \psi - \psi \partial_\nu \psi^*).$$

It turns out that the relations (29) or, in a more general form,

$$g^{1/4}(r_1)\rho(r_1) = g^{1/4}(r_2)\rho(r_2),$$

$$g^{1/4} g^{\mu\nu} \partial_\nu \rho(y) \Big|_{y=r_1} = g^{1/4} g^{\mu\nu} \partial_\nu \rho(y) \Big|_{y=r_2}, \quad (30)$$

imply the above physical assumptions and provide four necessary relations. On the top of that we have the normalization condition

$$\int_V |\psi|^2 dV = 1. \quad (31)$$

The equations (30) determine the discrete energy spectrum. Of course the results are strongly dependent on the values of parameters r_0 , r_1 , r_2 and r_3 . In order to compare the results with the available data, let us us specify these parameters as follows:

$$r_0 = 10 \text{ nm}, \quad r_1 = 54 \text{ nm}, \quad r_2 = 56 \text{ nm} \quad \text{and} \quad r_3 = 100 \text{ nm}. \quad (32)$$

Typically, the outer diameter of CNT ranges between 2 and 20 nm and inner diameter ranges between 1 and 3 nm, interlayer distance is 3.4 nm as it is established by the high-resolution TEM techniques. The values (32) correspond to the typical spacing between the layers for nanotubes, confirmed, in particular, by the experiments using diffraction

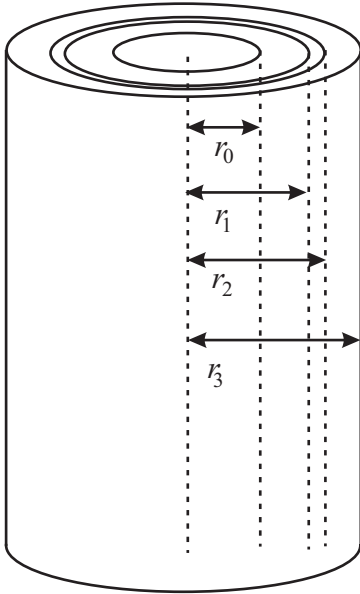


Figure 2: An illustration of the general geometrical form of a MWNT with the inner diameter of 20 *nm* and outer diameter of 200 *nm*.

and HRTEM image techniques [30, 31]. We consider here the possibility of describing MWNT, with several layers of carbon or other materials. Indeed, since we are looking for a qualitative correspondence with the results obtained by other methods, there is no much sense in performing calculations for large amount of possible nanotube diameters. However, since our method is really simple, such calculation can be easily performed, e.g., for any particular MWNT where the fast theoretical evaluation of the effect is needed. The system, as showed in Figure 2, can be treated geometrically, by identifying nanotubes with geometrical properties. In our consideration, a different kind of nanotube at $r = 55 \text{ nm}$ means a geometrical defect at the corresponding region.

Let us note that, taking the radius magnitude close to the ones which are typically found in nanosystems, including MWNT's, we also assume that the (e.g. carbon) nanotubes layers are of the same chirality. Indeed, one can suppose that a nanotube located at the middle, at $r = 55 \text{ nm}$, has different chirality, as well as, pehaps, few nanotubes in its vicinity [16].

Let us find the energy spectrum for the above choice, which depends on the quantum number m . We shall start from the fundamental state, $m = 0$. One can write equation (30) in terms of just one arbitrary constant, say, c_1 , which can be fixed by using the condition (31)). The corresponding equation is transcendental and rather cumbersome, so it is not convenient to write it here. The solution was performed with the help of the software *Mathematica* [32]. We have found the values for $\chi = \sqrt{2mE}/\hbar$ which are solutions of eq.

(30). The first three eigenvalues are placed in the left column of Table 1. For the purpose of comparison, we put the corresponding eigenvalues for the simplest case of the conducting cylinder without geometrical defect, in the right column. Similar results are presented in Table 2 for the $m = 1$ case.

χ (nm^{-1})	with defect ($l = 2nm$)	without defect ($l = 0nm$)
χ_1	0.03383	0.03314
χ_2	0.07016	0.06858
χ_3	0.10612	0.10377

Table 1: Energy spectrum for $m = 0$ with tube defect (left) and without defect (right).

The quantities χ_1 , χ_2 and χ_3 correspond to the first three energy eigenvalues.

From these results, one can see that the tube defect does shift, at the first place, the energy spectrum as a whole while it almost does not change the energy gap. Still there is a very small effect and the tendency is to reduce the gap slightly in all cases. Similar situation occurs for $m = 1$ (see Table 2). This shift depends on the size $l = r_2 - r_1$ of the cutting region. In Table 3, we put the first three energy eigenvalues for the cases $l = 0nm$, $l = -2nm$, $l = 2nm$ and $l = 4nm$, for $m = 0$. Of course, $l = 0$ corresponds to the case without defect. The case $l = -2nm$ corresponds to a negative tube dislocation (see Figure 1b).

χ (nm^{-1})	with defect ($l = 2nm$)	without defect ($l = 0nm$)
χ_1	0.04009	0.03941
χ_2	0.07490	0.07331
χ_3	0.10982	0.10748

Table 2: Energy spectrum for $m = 1$ with tube defect (left) and without defect (right).

It is remarkable that the energy levels do shift under the mapping from the “old” coordinates to the physical ones while one could naively expect that these levels remain the same. The reason is that (as we have already mentioned) the mapping does not change the *general* solutions of the Schrödinger equations, while our interest is concentrated on the particular solutions with the given boundary conditions. These conditions do change under the mapping and this makes the solutions of the equation (19) really nontrivial.

χ (nm^{-1})	$l = -2nm$	$l = 0nm$	$l = 2nm$	$l = 4nm$
χ_1	0.03248	0.03314	0.03383	0.03456
χ_2	0.06706	0.06858	0.07016	0.07183
χ_3	0.10153	0.10377	0.10612	0.10858

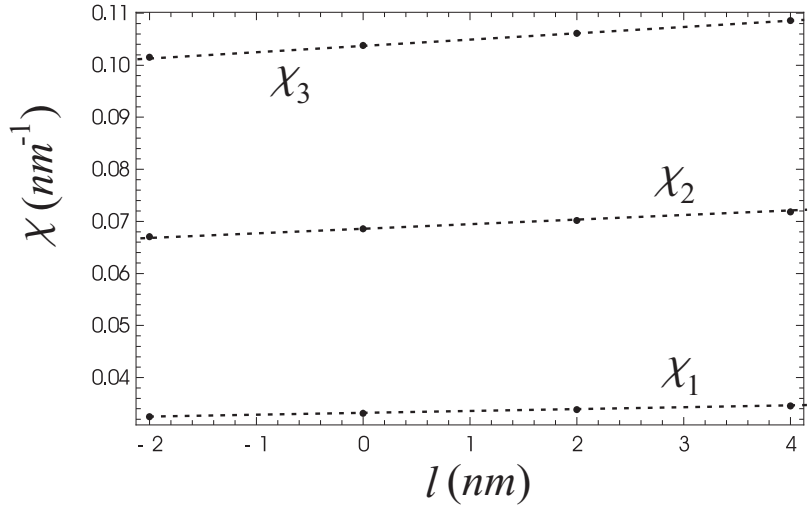


Figure 3: Representation of the data of Table 3 in the plane $\chi \times l$. The first three eigenvalues, χ_1 , χ_2 and χ_3 are plotted for the cases $l = -2 nm$, $l = 0 nm$, $l = 2 nm$ and $l = 4 nm$. The dashed lines are supposed to describe the assumed linear dependence.

Table 3: The three first energy levels for $m = 0$ for the cases $l = -2 nm$, $l = 0 nm$, $l = 2 nm$ and $l = 4 nm$.

How is the dependence of the energy levels on the size l ? As suggested by the data of Tables 1, 2 and 3, positive l induces a slight increase of energy eigenvalues, while a negative l lowers them. The exact function $\chi_i(l)$ ($i = 1, 2, 3$) is unknown and all we can do is to plot the data from Table 3 as shown in Figure 3. This plotting clearly suggests a linear dependence between the energy levels χ and the size l .

One can notice, by straightforward computation, that the energy gaps, $\Delta\chi_1 := \chi_2 - \chi_1$ and $\Delta\chi_2 := \chi_3 - \chi_2$, are slightly increased for $l > 0 nm$ and decreased for $l < 0 nm$. For example, for $l = 4 nm$, $\Delta\chi_2$ is 4.4% greater than the corresponding value of $\Delta\chi_2$ for $l = 0 nm$. The values of $\Delta\chi_{1,2}$ are shown in Table 4, and are plotted in Figure 4. We can observe again a linear relation between $\Delta\chi$ and l . Let us notice that, by assuming linear dependence, the straight line describing $\Delta\chi_1(l)$ has a lower angular coefficient than the one corresponding to $\Delta\chi_2(l)$.

$\Delta\chi$ (nm^{-1})	$l = -2 nm$	$l = 0 nm$	$l = 2 nm$	$l = 4 nm$
$\Delta\chi_1$	0.03458	0.03544	0.03633	0.03727
$\Delta\chi_2$	0.03447	0.03520	0.03596	0.03675

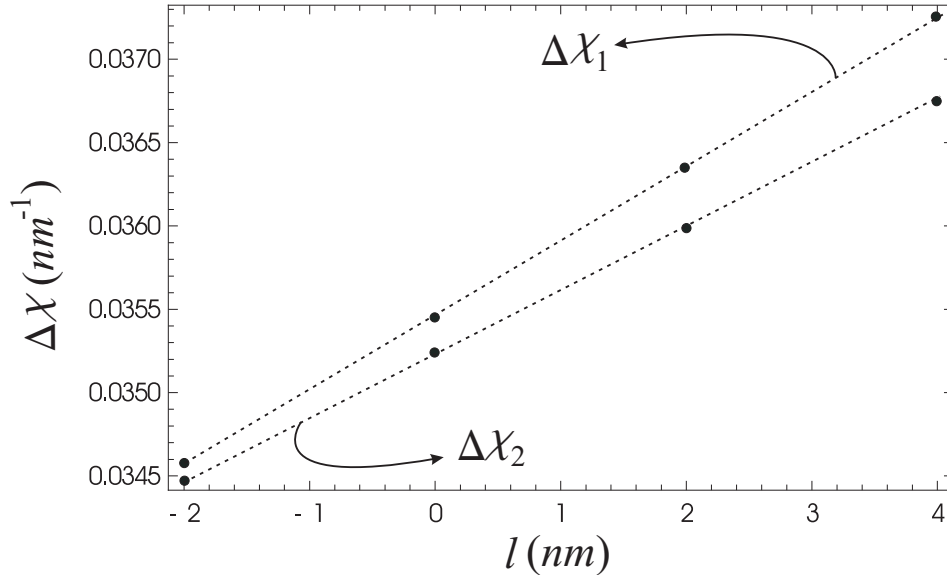


Figure 4: Representation of the data of Table 4 in the plane $\Delta\chi \times l$. The two first energy gaps, $\Delta\chi_1 = \chi_2 - \chi_1$ and $\Delta\chi_2 = \chi_3 - \chi_2$, are drawn for different values of l . The dashed lines are supposed to describe the assumed linear dependence.

Table 4: The first two energy gaps, $\Delta\chi_1 = \chi_2 - \chi_1$ and $\Delta\chi_2 = \chi_3 - \chi_2$, for $m = 0$ for different values of l .

4.2 Density Curves

In the ideal gas approximation, the volume integral of the density distribution, $\int \sqrt{g} |\psi(y, \phi, z)|^2 d\phi dz dr$, is proportional to $\int y |\rho(y)|^2 dr$, with the constant of proportionality having dimensions of area. From the condition (31), $|c_1|^2$ has dimensions of $[\text{length}]^{-3}$ and one can find (using *Mathematica* software) the following values for $|c_1|^{-2}$: 2265.29 nm^3 , 8985.42 nm^3 and 8151.17 nm^3 for χ_1 , χ_2 and χ_3 , respectively, for $m = 0$, with tube defect. The corresponding values without defect, for χ_1 , χ_2 and χ_3 are 2315.70 nm^3 , 8017.33 nm^3 and 11471.10 nm^3 , respectively.

With these values, one can plot the normalized density against the coordinate y . In Figure 5, for the lowest energy eigenvalue, χ_1 , and $m = 0$, the normalized density is plotted as well as the normalized density without defect for comparison. Notice that the curve in the presence of defect has a cut because the point r_1 is identified with r_2 , so the interval $r_1 < y < r_2$ is formally absent in the space with tube defect. The defect raises density in the central region. It is interesting to observe that this is not the unique effect caused by the defect. With the help of the *Mathematica* software, one can calculate the value of y for

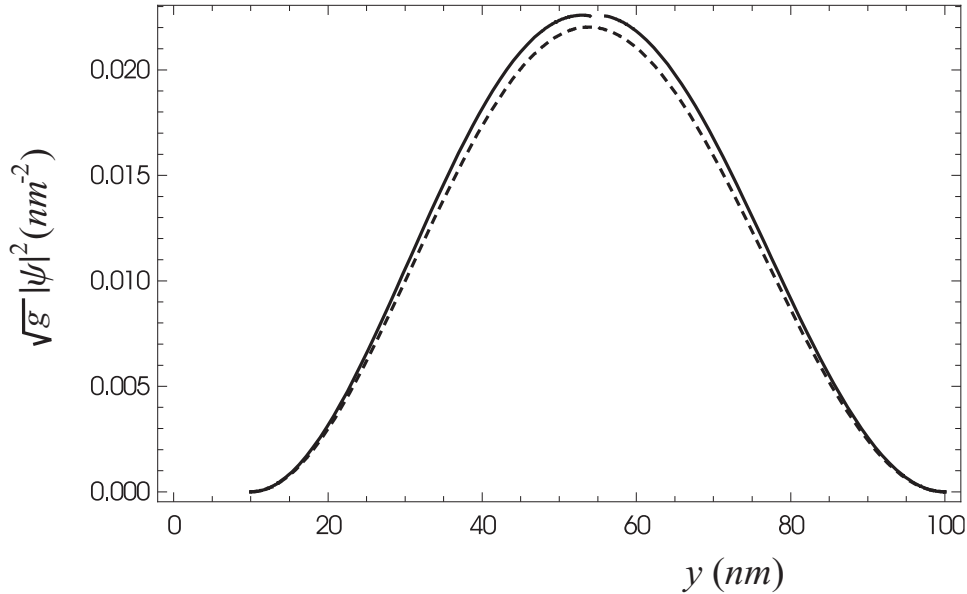


Figure 5: Normalized density for $m = 0$ and $\chi = \chi_1$. The continuous line has a cut and describes density in the presence of tube defect. The dashed line describes density without defect.

which the density reaches its maximum value. This value is given by $y_{\max} \approx 53.80 \text{ nm}$ for the density without defect and $y_{\max} \approx 52.95 \text{ nm}$ for the density with $m = 0$ and $l = 2 \text{ nm}$. Thus, the defect not only raises the density distribution, but it also drags its peak to the left.

Let us remark that the curves describing the particle density have not symmetry around the straight line $y = 55 \text{ nm}$. The peaks of the curves in Figure 5 are localized in the left half of the region $10 \text{ nm} \leq y \leq 100 \text{ nm}$, and not in the middle of it. Actually, this property is essentially related to the properties of the Bessel functions. Indeed, let us remember that the system is not unidimensional, such that it does not possess symmetry around the middle point.

For $\chi = \chi_2$ and still $m = 0$, the corresponding density curves are plotted in Figure 6. In the presence of the tube defect, the density is lower in central region but greater in the marginal regions, $y \approx 30 \text{ nm}$ and $y \approx 80 \text{ nm}$. The shifts in the density distribution are small and of the same order in both cases, χ_1 and χ_2 , but in the last case the difference is richer. In the central region, the defect raises the density for $\chi = \chi_1$ and lowers the density for $\chi = \chi_2$. Of course, for a larger l , these effects may become much more sensitive.

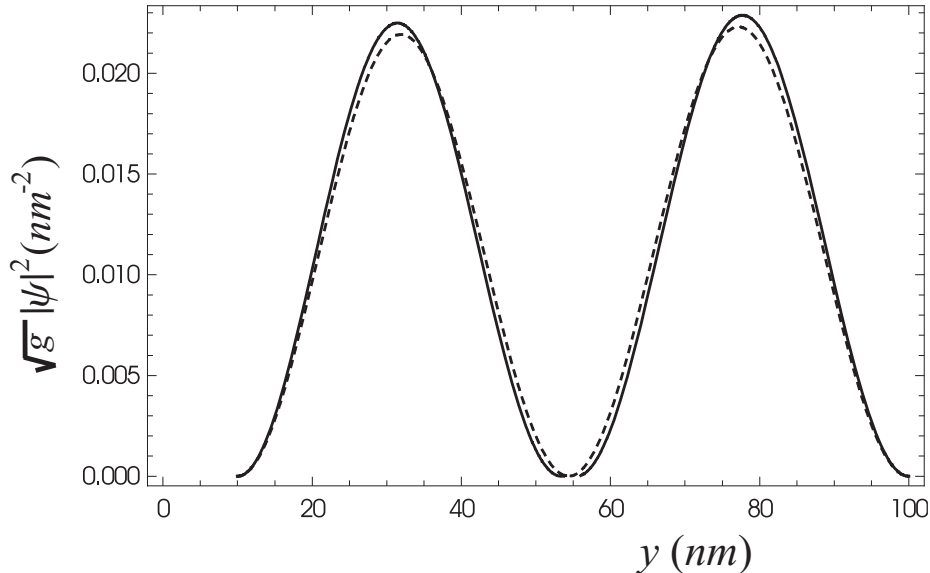


Figure 6: Normalized density for $m = 0$ and $\chi = \chi_2$. The continuous line has a cut and describes density in the presence of tube defect. The dashed line describes density without defect.

5 Conclusions

We considered the solution of the Schrödinger equation in the restricted region of space with cylindrical geometric defect. The region is confined between the two cylindrical shells and the diameter of the defect is intermediate between the ones of these shells. Geometrically this configuration resembles the double-wall nanotube (DWNT) and, therefore, it can be regarded as a simplified model of such nanotube. Due to the fact that the electron can freely move within the space between the two border shells, one can associate the system with the M/M-type DWNT. The solution of the Schrödinger equation shows the influence of the geometric defect on the energy gap and charge distribution. In particular, one meets a modified energy spectrum and the distribution of charge density, in the ideal gas approximation. These effects are qualitatively similar to the ones previously reported for some MWNTs in [18], where the calculations were based on the tight-binding method. In this respect we can conclude that the approach based on geometric defects, which does not take into account anything but the general form of the DWNT, is able to provide some (very restricted, indeed) information about the electron behaviour.

It is obvious that the method based on geometric defects can not compete with the standard approaches based on molecular dynamics. The reason is that the geometric defects method can not take into account full details of the structure of the compound and is, in some sense, too general. At the same time this method may become much more interesting if one develops it further and, in particular, learns how to deal with more

sophisticated versions of geometric defects. In particular, it looks possible to take into account the chirality of the nanotube and, also, include the external magnetic field. We expect to consider these issues elsewhere.

Acknowledgments

G.B.P., E.K. and I.Sh. are indebted to CNPq, FAPEMIG and FAPES for partial support. M.K. is thankful to FAPEMIG for support of his visit to Brazil and to the Physics Department of the Universidade Federal de Juiz de Fora for warm hospitality. Also, he thanks the Russian Foundation of Basic Research (Grant No. 08-01-00727), and the Program for Supporting Leading Scientific Schools (Grant No. NSh-3224.2008.1) for financial support. The work of I.Sh. has been also supported by ICTP.

References

- [1] P.M. Chaikin and T.C. Lubensky, *Principles of Condensed Matter Physics*. (Cambridge University Press, Cambridge, 2000).
- [2] M. Kleman and J. Friedel, *Rev. Mod. Phys.* 80 (2008) 61.
- [3] M. O. Katanaev and I. V. Volovich. Theory of defects in solids and three-dimensional gravity. *Ann. Phys.*, 216(1):1–28, 1992.
- [4] M. O. Katanaev and I. V. Volovich. Scattering on dislocations and cosmic strings in the geometric theory of defects. *Ann. Phys.*, 271: 203–232, 1999.
- [5] M. O. Katanaev. Geometric theory of defects. *Physics – Uspekhi*, 48(7):675–701, 2005.
- [6] G. de Berredo-Peixoto and M. O. Katanaev, *Tube dislocations in gravity*, *J. Math. Phys.* 50: 042501, 2009.
- [7] W.H. Zurek, *Physics Reports*, 276 (1996) 177;
T. W. B.Kibble and G.R. Pickett, *Philosophical transactions of the Royal Society A - Mathematical, Physical and Engineering Sciences*, 366 (2008) 2793.
- [8] M. Das, A. Vaziri, A. Kudrolli, and L. Mahadevan, *Curvature Condensation and Bifurcation in an Elastic Shell*, *Phys. Rev. Lett.* 98: 014301, 2007.
- [9] D.L. Cheung and M.P. Allen, *Forces between Cylindrical Nanoparticles in a Liquid Crystal* *Langmuir*, 24 (2008) 1411.

- [10] T.W. Ebbesen (Editor), *Carbon Nanotubes. Preparation and Properties*. CRC Press, Boca Raton New York London Tokyo, 1997.
- [11] R. Saito, G. Dresselhaus and M.S. Dresselhaus, *Physical Properties of Carbon Nanotubes*, (Imperial College, London, 1998).
- [12] P.J.F. Harris, *Carbon Nanotubes and Related Structures: New Materials for the Twenty-First Century*, (Cambridge University Press, 1999).
- [13] M. S. Dresselhaus, G. Dresselhaus and P. Avouris (Editors), *Carbon Nanotubes : Synthesis, Structure, Properties, and Applications*, (Springer-Verlag, 2000).
- [14] A. M. Fennimore, T. D. Yuzvinsky, Wei-Qiang Han, M. S. Fuhrer, J. Cumings, A. Zettl, *Rotational actuators based on carbon nanotubes*, Nature **424** (2003) 408;
 A. Modi, N. Koratkar, E. Lass, B. Wei, P.M. Ajayan, *Miniaturized gas ionization sensors using carbon nanotubes*, Nature **424** (2003) 171;
 M. Zhang, S. Fang, A.A. Zakhidov, S.B. Lee, A.E. Aliev, C.D. Williams, K.R. Atkinson, and R.H. Baughman, *Strong, Transparent, Multifunctional, Carbon Nanotube Sheets*, Science **309** (2005) 1215;
 R.H. Baughman, A.A. Zakhidov, and W.A. de Heer, *Carbon Nanotubes—the Route Toward Applications*, Science **297** (2002) 787;
- [15] T. Shimada, T. Sugai, Y. Ohno, S. Kishimoto, T. Mizutani, H. Yoshida, T. Okazaki and H. Shinohara, Appl. Phys. Lett. **84** (2004) 2412.
- [16] Z. Xu, X. Bai, Z.L. Wang and E. Wang, *Multiwall Carbon Nanotubes Made of Monochirality Graphite Shell*, J. Am. Chem. Soc. **128** (2006) 1052.
- [17] F. Villalpando-Paez, H. Son, D. Nezich, Y.P. Hsieh, J. Kong, Y.A. Kim, D. Shimamoto, H. Muramatsu, T. Hayashi, M. Endo, M. Terrones and M.S. Dresselhaus, Nano Lett. **8** (2008) 3879.
- [18] Y. H. Ho, G. W. Ho, S. J. Wu, and M. F. Lin, J. Vac. Sci. Technol. B **24**(3) (2006) 1098.
- [19] J. Gravesen, M. Willatzen and L. C. Lew Yan Voon, J. Math. Phys. **46**: 012107, 2005.
- [20] D. V. Long and G. M. Shore, Nucl. Phys. **B 530**: 247-278, 1998.
- [21] A. Mostafazadeh, Phys. Rev. **A 54**: 1165-1170, 1996.
- [22] S. Azevedo, Mod. Phys. Lett. **A 17**: 1263-1268, 2002.

- [23] C. A. L. Ribeiro, C. Furtado and F. Moraes, *Mod. Phys. Lett. A* **20**: 1991-1996, 2005.
- [24] P. Hohenberg, W. Kohn, *Phys. Rev.*, 136 (1964) B864;
 W. Kohn, L.J. Sham, *Phys. Rev.*, 140 (1965) A1133;
 W. Kohn, M.C. Holthausen, *A Chemists Guide to Density Functional Theory*,
 (WILEY-VCH, Second Edition, 2001).
- [25] L. D. Landau and E. M. Lifshits. *Theory of Elasticity*. Pergamon, Oxford, 1970.
- [26] We put the word “induced” in inverted commas because on the cutting surface the induced metric is not defined.
- [27] M. O. Katanaev. Wedge dislocation in the geometric theory of defects. *Theor. Math. Phys.*, 135(2):733–744, 2003.
- [28] M. O. Katanaev. One-dimensional topologically nontrivial solutions in the Skyrme model. *Theor. Math. Phys.*, 138(2):163–176, 2004.
- [29] Both features may not hold in the spinning particle case, which becomes relevant for the more general types of tube geometric defects.
- [30] T.W. Ebbesen (Editor), *Carbon Nanotubes. Preparation and Properties*. (CRC Press, Boca Raton, 1997), see especially Chapter 3 therein,
 P.M. Ajayan, *Structure and Morphology of Carbon Nanotubes*.
- [31] M.S. Dresselhaus, G. Dresselhaus and P.C. Eklund, *Science of Fullerenes and Carbon Nanotubes*, (Academic Press, San Diego, 1996), see especially the data in Chapter 19.
- [32] S. Wolfram, *The Mathematica Book* (Cambridge Univ. Press, 1999), the M6 version has been used here.